"Good-but-Imperfect" Electromagnetic Reverberation in a VIRC

Ramiro Serra [*1], Frank Leferink [*‡2], Flavio Canavero [†3]

[*] *University of Twente, Enschede, The Netherlands.*
[1] r.serra@ewi.utwente.nl
[2] frank.leferink@utwente.nl

[‡] *Thales Nederland B.V., Hengelo, The Netherlands.*
[2] frank.leferink@nl.thalesgroup.com

[†] *Politecnico di Torino, Turin, Italy.*
[3] flavio.canavero@polito.it

***Abstract*—Novel theoretical probability density functions (PDF) of electromagnetic fields inside reverberation chambers operating in a "good-but-imperfect" regime have been recently reported. The present work reports on the application and assessment of these PDFs using a non-conventional type of reverberation chamber, namely the Vibrating Intrinsic Reverberation Chamber (VIRC). A vector network analyzer was used in order to measure the complex field components. An electrically short dipole antenna was used as a receiving antenna. Five thousand frequency points were taken ranging from 200 MHz (undermoded regime) to 4 GHz (overmoded regime), so one measurement every 760 kHz was performed. For each frequency, 200 samples of the real and imaginary part of the field were measured. Measurements confirm the fact that the novel PDFs are able to describe the occurrence of anomalous statistics in the VIRC.**

I. Introduction

A Reverberation Chamber (RC) consists of a metallic shielded room of finite conductivity with a stirring device, antennas, an equipment under test, and other devices inside. It formally can be defined as an electrically large, high Q, *multimoded* cavity using mode stirring to create changing boundary conditions in order to obtain a statistically uniform electromagnetic field [1].

RCs are gaining significant confidence in their use for electromagnetic compatibility measurements and multipath environment characterization. The correct interpretation of the measurement results and the performance optimization of RCs require a full understanding of their working principles.

A particular non-conventional example of a RC is the one referred to as the Vibrating Intrinsic Reverberation Chamber (VIRC) [2]. The VIRC is a chamber with an intrinsically complex geometry where wave diffusion is given by the naturally jagged surface of the flexible walls. Moreover, it is not only a complex-shaped chamber but also a vibrating one, thus changing the mode structure at every stir state, which in this case is a particular configuration of the chamber shape. The practical means for realizing such a chamber is basically to construct a shielded room with flexible conductive material and make the whole structure vibrate.

It has been reported that most statistical models in reverberation chamber theory assume ideal reverberation conditions. When using high-power goodness of fit tests and with a large number of samples, it can be seen that in real RCs it is not so simple to find ideal reverberant conditions for every frequency, even in the overmoded regime. The marginal PDFs reported before in [3] fit better the real measured data than the *asymptotic* $\chi^{(2)}_{2\nu}$ distributions i.e. the theoretical ones for ideal reverberation.

The marginal distributions were validated in [3] using measurements provided by two conventional RCs: the one of Alenia Aeronautica in Caselle, Italy and the one of IETR-INSA in Rennes, France. This paper aims at applying this statistical model to the VIRC. The VIRC represents a more suitable environment as a random field generator than conventional RCs [4].

II. Good-but-Imperfect Reverberation

Main statistical models for reverberation chambers (e.g. [1], [5]) conclude that each complex part of the Cartesian field components $E_{\alpha\beta}$, where $\alpha = x, y, z$ represents the Cartesian component and $\beta = r, i$ the real and imaginary part, respectively, is normally distributed [6] with zero mean. The statistical distribution of complex fields that represent ideal reverberation inside a perfect enclosure can then be deduced from ideal circular Gauss normal variates resulting in well-known distributions. The magnitude is found to be $\chi_{2\nu}$ distributed, the energy density is $\chi^2_{2\nu}$ distributed for a Cartesian field component ($\nu = 1$) or total field ($\nu = 3$) and the phase $U(-\pi, \pi)$ (uniformly) distributed.

Nevertheless, just by ensuring Gauss-normal field components does not guarantee that the known *asymptotic* distributions $\chi^{(2)}_{2\nu}$ can always be found. Other assumptions must be taken as conditions, such as that the complex Cartesian field components are unbiased, independent and identically distributed Gauss-normal variates, i.e. with zero mean ($\mu_{E_{\alpha r}} = \mu_{E_{\alpha i}} = 0$), equal variance ($\sigma^2_{E_{\alpha r}} = \sigma^2_{E_{\alpha i}}$) and no correlation between them ($\rho_{E_{\alpha r}\, E_{\alpha i}} = 0$). It has been stated that in real

RCs, even at relatively high frequencies, these ideal conditions are often not met [3].

Experiments were carried out in a VIRC [4] at the Environmental Competence Center of Thales Nederland in Hengelo, The Netherlands, using a vector network analyzer and a short dipole antenna in order to measure the complex field components. The size of the VIRC is 1 m $\times$ 1.2 m $\times$ 1.5 m. The first resonant frequency is around $f_{110} = 160$ MHz (its value changes depending on the tightness in which the VIRC is fixed). According to the generally accepted criteria (like e.g. in [7]) the lowest useable frequency (LUF) might lay between 480 MHz and 960 MHz. For each frequency, 200 samples were measured while the VIRC was shaking and performing mode-stirring. Different statistical tests were applied to the measured data in order to test the above mentioned assumptions.

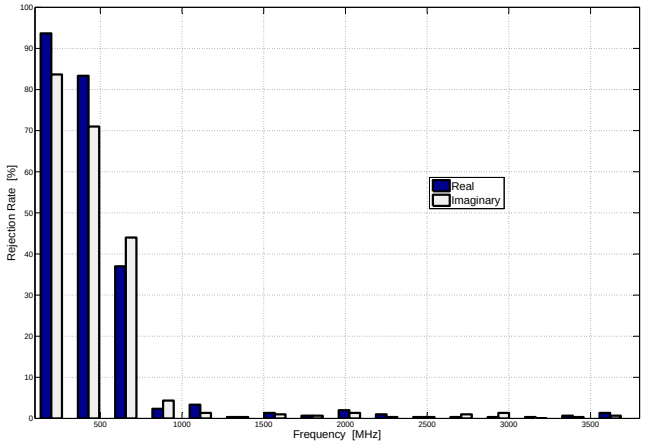

Fig. 1. Rejection rates for the Anderson-Darling GoF test for measurements performed in a VIRC for the real and the imaginary part of field.

Figure 1 shows the rejection rates (percentage of rejected tests over a frequency bin) for the Anderson-Darling [8] Goodness-of-Fit (GoF) test for the real and the imaginary part of the field measured in a VIRC, for a 5% of confidence level. It can be seen that the rejection rate is rather low (significantly lower than 5%) for the overmoded region.

The Student's t-distribution helped in testing the hypothesis of zero-mean (T-test), equal variances (F-test) and uncorrelation (Pearson's ρ test), all of them for a 5 % of confidence level. Figure 2 shows the rejection rates resulting from the measurements performed in the VIRC. It can be seen that in this case, the rejection rates are significantly high.

As an example of the concepts explained above, let us consider two measurements, one at 3.612 GHz and the other one at 3.63 GHz. Both measurements were chosen for frequencies in the overmoded regime. Their histograms with superimposed fitted normal PDFs can be seen in Fig. 3. The dashed vertical lines indicate, the average value (in the middle) and the average plus or minus the standard deviation at its sides.

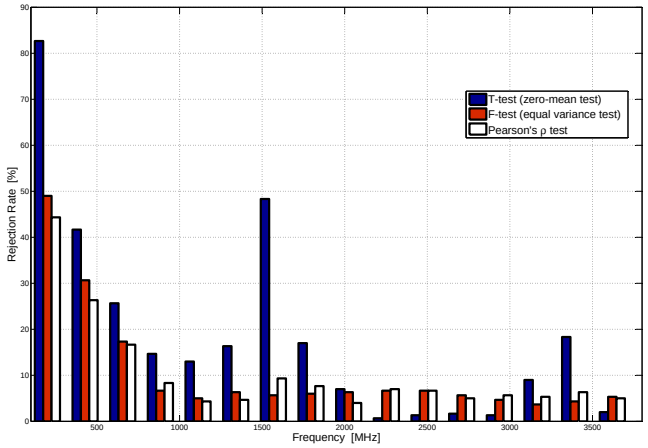

Fig. 2. Testing some basic assumptions on the first- and second-order statistical properties of the real ($E_{\alpha r}$) and imaginary ($E_{\alpha i}$) part of the field components. Rejection rates show the percentage of rejected tests over frequency bins.

The GoF applied to the sets of data in Fig. 3(a), gave p-values of 0.31 and 0.14 for the real and the imaginary part, respectively; while for the data in Fig. 3(b), the p-values resulted in 0.92 and 0.23. This gives good reason to accept the hypotheses of normality on the four cases.

Nevertheless, there is a difference between the two data sets and it is that in the case of Fig. 3(a), the T-test, the F-test and the Pearson's ρ test failed to accept the null hypotheses of zero-mean, equal variances and uncorrelation, respectively; while the data in Fig. 3(b) did not fail.

The specific problem that will be treated in the present paper assumes that *asymptotic* Gauss normal distributions for the field components apply, but the overall operational conditions depart from ideality. This condition has been referred to as the "good-but-imperfect" reverberation [3]. In this sense, data of Fig. 3(a) can be considered as an example of "good-but-imperfect" reverberation, while data on Fig. 3(b) are closer to the ideal situation.

III. Model Overview

The derivation of the statistical model in [3] is based on considering two gaussian random variables with mean values, variances and correlation between them that are departed from the ideal assumptions. A bivariate approach using a complete joint gaussian distribution of these variables is defined.

For our model formulation we start considering the joint PDF of two Gauss-normal random variables ξ and η [6]:

$$f_{\xi\eta}(\xi,\eta) = \frac{1}{2\pi\sigma_\xi\sigma_\eta\sqrt{1-\rho^2}}\cdot \cdot e^{\frac{-1}{2(1-\rho^2)}\left(\frac{(\xi-\mu_\xi)^2}{\sigma_\xi^2}+\frac{(\eta-\mu_\eta)^2}{\sigma_\eta^2}-\frac{2\rho(\xi-\mu_\xi)(\eta-\mu_\eta)}{\sigma_\xi\sigma_\eta}\right)}, \quad (1)$$

where μ_ξ and μ_η are the mean values for ξ and η, respectively, σ_ξ^2 and σ_η^2 are the corresponding variances and ρ is the correla-

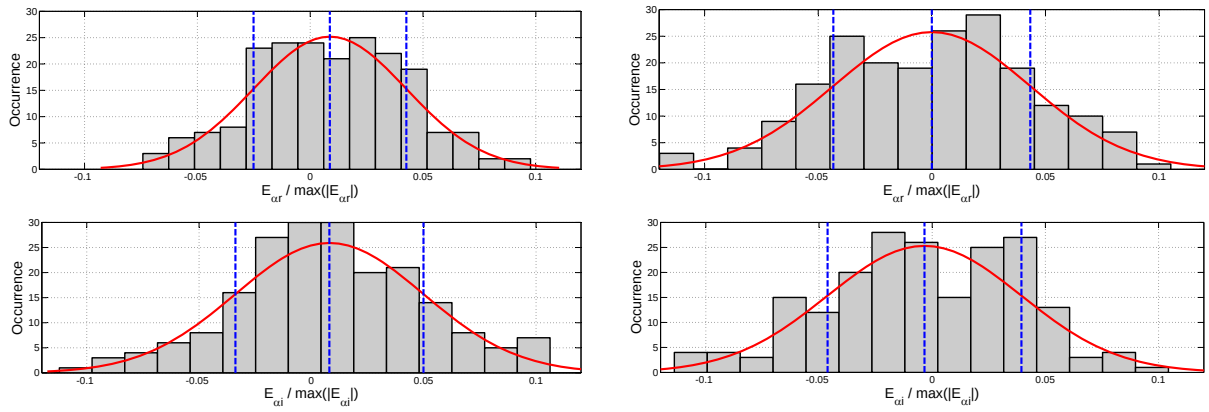

(a) Measurements at 3.612 GHz

(b) Measurements at 3.63 GHz

Fig. 3. Histogram with superimposed fitted normal density for the real and imaginary part of the (normalized) electric field (upper and bottom panel, respectively). Measurements were performed for two frequencies in the overmoded regime.

tion coefficient between ξ and η as defined in [6]. The function $f_{\xi\eta}(\xi,\eta)$ of (1) will be denoted by $N(\mu_\xi,\mu_\eta;\sigma_\xi,\sigma_\eta;\rho)$.

It can be seen in Fig. 4 three-dimensional histograms of the bivariate measured data, with the fitted bivariate joint gaussian distribution of eq. (1). A three-dimensional histogram simply counts the number of points laying in the two dimensional bins in which the variates are divided.

A change of variables representing each field component in terms of its magnitude and phase, leads us to consider a new pair of random variables:

$$r = |E_\alpha| = \sqrt{\xi^2+\eta^2} \qquad \phi = \arg E_\alpha = \arctan\frac{\eta}{\xi}, \tag{2}$$

where $r \geq 0$ and $-\pi < \phi \leq \pi$. With this assumption, the system in (2) has a unique solution

$$\xi = r\cos\phi \qquad \eta = r\sin\phi \qquad \text{for} \qquad r \geq 0. \tag{3}$$

Since the Jacobian of this variable transformation is simply

$$J_{\xi\eta r\phi}(r,\phi) = \begin{vmatrix} \cos\phi & \sin\phi \\ -r\sin\phi & r\cos\phi \end{vmatrix}^{-1} = \frac{1}{r}, \tag{4}$$

we conclude that the joint PDF of the new set of variables in (2) is

$$f_{r\phi}(r,\phi) = r f_{\xi\eta}(r\cos\phi, r\sin\phi) \qquad r \geq 0, \tag{5}$$

and zero for $r < 0$. This result is readily obtained extending the procedure illustrated in [6].

Figure 5 shows the three-dimensional histograms of the same measurements of Fig. 4, but with the change of variables in (2) applied to them. The fitted joint PDF of eq. (5) is also superimposed.

The PDFs of the individual magnitude and phase of the field components can be derived as the marginal distributions of the joint $f_{r\phi}(r,\phi)$ of eq. (5) by calculating:

$$f_r(r) = \int_{-\pi}^{\pi} f_{r\phi}(r,\phi)\,d\phi \qquad f_\phi(\phi) = \int_0^{\infty} f_{r\phi}(r,\phi)\,dr. \tag{6}$$

Figure 6 shows the histograms and the marginal PDFs of eq. (6) for the magnitude and phase of the (normalized) electric field of the present example. Also the PDFs for ideal conditions of operation (Rayleigh for the magnitude and Uniform for the phase) are present in the figure for comparison. It can be seen that the distribution of the phase is significantly more disturbed by the imperfections than the distribution of the magnitude. Let us recall that both these sets of measurements embed reasonably good Gauss-normal variates.

A. Summary

The sequence of the operations defined above will be summarized and presented in this subsection for clarity.

1) We start considering two random variables ξ and η, normally distributed with:

$$f_\xi(\xi) \sim N(\mu_\xi,\sigma_\xi)\,,$$
$$f_\eta(\eta) \sim N(\mu_\eta,\sigma_\eta)\,,$$

where μ_ξ and μ_η are the mean values for ξ and η, respectively, σ_ξ^2 and σ_η^2 are the corresponding variances. The variables are correlated with correlation ρ. Figure 3 shows an example of two pairs of data samples with this description.

2) Secondly, consider the joint distribution between ξ and η of eq. (1). The distributions of ξ and η can easily be "retrieved" by doing:

$$f_\xi(\xi) = \int_{-\infty}^{\infty} f_{\xi\eta}(\xi,\eta)\,d\eta \qquad f_\eta(\eta) = \int_{-\infty}^{\infty} f_{\xi\eta}(\xi,\eta)\,d\xi\,.$$

Figure 4 shows the bivariate PDF applied to the measurements following this process.

3) Thirdly, apply the change of variables in eq. (2) that results in the joint PDF of eq. (5). This change of variables represent a change of coordinates from rectangular to polar representation of the complex [electric field]

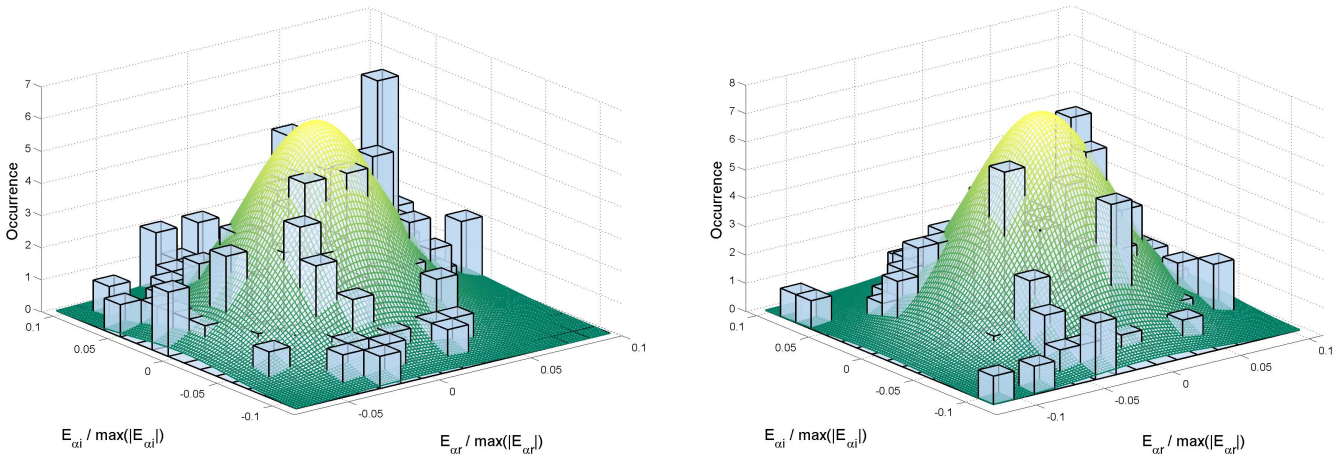

(a) Measurements at 3.612 GHz

(b) Measurements at 3.63 GHz

Fig. 4. Three-dimensional histogram with superimposed fitted bivariate normal density function. Measurements were performed for two frequencies in the overmoded regime.

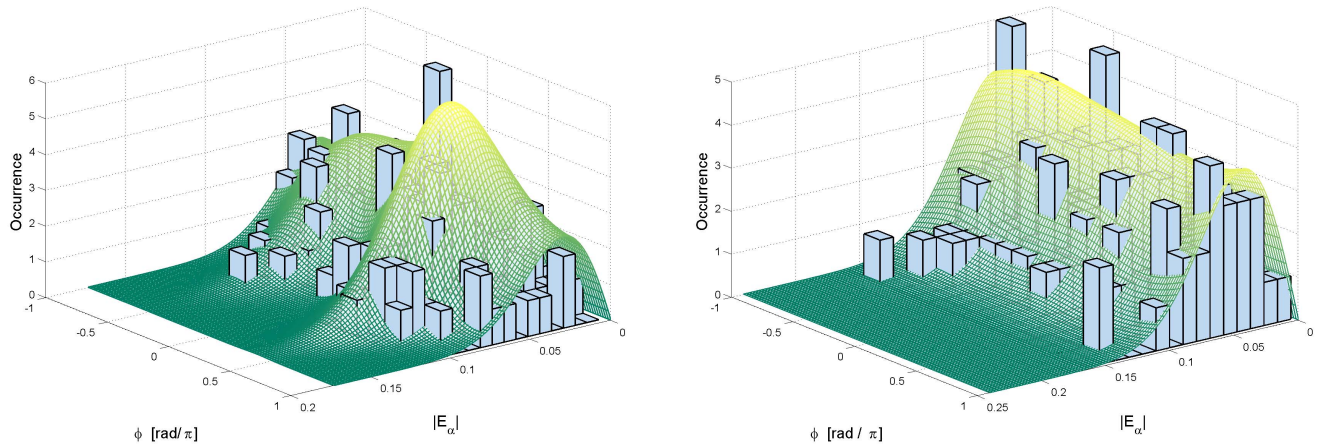

(a) Measurements at 3.612 GHz

(b) Measurements at 3.63 GHz

Fig. 5. Three-dimensional histogram with superimposed fitted joint PDF of eq. (5). Measurements were performed for two frequencies in the overmoded regime.

vector. Figure 5 shows how data is transformed with this procedure.

4) Finally, find the distribution of r and ϕ as the marginal distribution of eq. (5) by applying eq. (6). Figure 6 shows the final result of the process.

In the following section, the marginal distributions of eq. (6) obtained by integration of a two-dimensional joint PDF are compared with theoretical PDFs for ideal situations.

IV. Results

A Rohde & Schwarz ZVA40 Vector Network Analyzer (VNA) was used in order to measure the complex field components. An electrically short dipole antenna was used as a receiving antenna. The electrically short dipole antenna is necessary for sampling a (rectangular) component of the electric field. The receiving antenna was placed in the geometrical center of the working volume, oriented along the longest dimension of the working volume. Five thousand frequency points were taken ranging from 200 MHz (undermoded) to 4 GHz (overmoded), so one measurement every 760 kHz was performed. For each frequency, 200 samples of the real and imaginary part of the field were measured. A full VNA calibration has been done over the entire frequency band.

Figure 7 shows the rejection rates of the Anderson-Darling GoF test with the marginal and with the ideal distributions for measurements performed in the VIRC for the magnitude and phase. Appropriate critical values for these particular PDFs need to be derived. We assume a commonly used critical value of 0.752 for a 5% level of confidence test. Looking for more adapted critical values goes beyond the aim of the present work and may not have a significant consequence on our validation results. The better fit (lower rejections rates) can be found as well for the VIRC as it was found for conventional RCs [3].

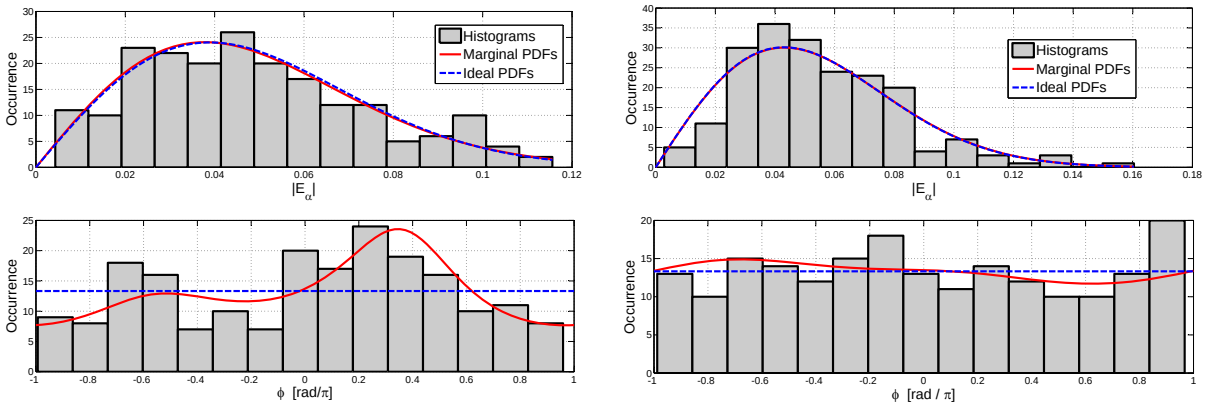

(a) Measurements at 3.612 GHz

(b) Measurements at 3.63 GHz

Fig. 6. Histograms with superimposed fitted marginal PDFs of eq. (6) and ideal PDFs (Rayleigh and Uniform) for the magnitude and phase part of the (normalized) electric field (upper and bottom panel, respectively). Measurements were performed for two frequencies in the overmoded regime.

These marginal PDFs can give better reason for departures from ideality in well-performing RCs, situation that has been called "good-but-imperfect". In particular, the departure of the phase from a uniform distribution is noteworthy.

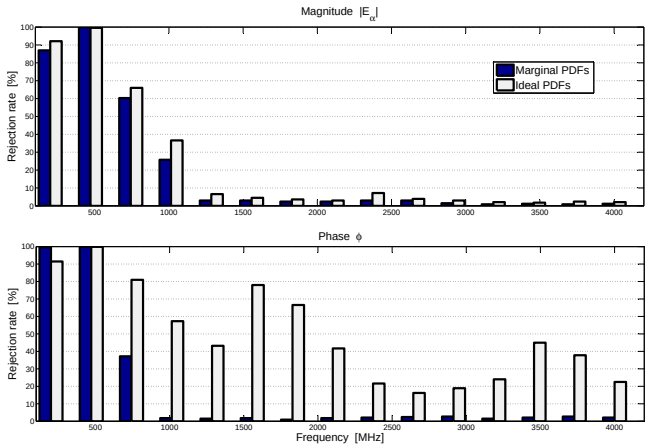

Fig. 7. Rejection rate of Rayleigh and Marginal PDFs for the magnitude (upper panel) and for Uniform and Marginal for the phase (bottom panel) of the electric field. Data refer to measurements in the VIRC.

V. Anomaly Classification

In the past sections we introduced and investigated a family of anomalous statistics occurring in the overmoded regime. The model applied in the present work allows us not only to detect these anomalies, but also to classify them. As explained in section III, three basic assumptions were relaxed in order to derive the marginal PDFs for "good-but-imperfect" reverberation. Each one of these assumptions specifies a different type of deviation from ideality. Eight different combinations of marginal PDFs can then be defined, by combining the zero-mean, equal variances and/or uncorrelated variates assumptions. In this manner, a number of alternative bivariate PDFs for the general elliptical Gaussian function of eq. (1) are therefore available accounting for different deviations from ideality:

$$
\begin{aligned}
&\text{Type I} && :f_{\xi\eta}(\xi,\eta) \sim N(0,0;\sigma,\sigma;0)\\
&\text{Type II} && :f_{\xi\eta}(\xi,\eta) \sim N(\mu_\xi,\mu_\eta;\sigma,\sigma;0)\\
&\text{Type III} && :f_{\xi\eta}(\xi,\eta) \sim N(0,0;\sigma_\xi,\sigma_\eta;0)\\
&\text{Type IV} && :f_{\xi\eta}(\xi,\eta) \sim N(\mu_\xi,\mu_\eta;\sigma_\xi,\sigma_\eta;0)\\
&\text{Type V} && :f_{\xi\eta}(\xi,\eta) \sim N(0,0;\sigma,\sigma;\rho)\\
&\text{Type VI} && :f_{\xi\eta}(\xi,\eta) \sim N(\mu_\xi,\mu_\eta;\sigma,\sigma;\rho)\\
&\text{Type VII} && :f_{\xi\eta}(\xi,\eta) \sim N(0,0;\sigma_\xi,\sigma_\eta;\rho)\\
&\text{Type VIII} && :f_{\xi\eta}(\xi,\eta) \sim N(\mu_\xi,\mu_\eta;\sigma_\xi,\sigma_\eta;\rho)
\end{aligned}
$$

Type I represents the ideal case. Type II accounts only for the case of nonzero-mean variates, i.e. resulting in the Rice distribution for the magnitude, as shown in [3]. Type III accounts for nonequal variances. And the list of eight types completes by adding more and more deviations from ideality. Two marginal PDFs per each type can be derived, resulting in a family of sixteen different PDFs, half of them for the magnitude, half for the phase of the electric field. The physical parameters $\mu_\xi, \mu_\eta, \sigma_\xi, \sigma_\eta$ and ρ are found to be acting as "shape parameters" (somehow similar to the k parameter for the Weibull), and from this fact comes the ability of the marginal PDFs of shape-changing and fitting better to measured data.

The parameters $\mu_\xi, \mu_\eta, \sigma_\xi, \sigma_\eta$ and ρ can be measured. A procedure of hypothesis-testing can be applied to decide whether a particular parameter can be accepted to as ideal or not, yielding the classification of distribution shapes into types I . . . VIII. In this manner, these parameters act as "classifiers". By means of this method we are able to characterize and analyze the statistical structure of anomalous occurrences.

Figure 8 shows the percentage of occurrence of each type over frequency bins. A total of 50 bins for the whole frequency

band were defined, resulting in 100 measured data sets in a band of 76 MHz per bin. The percentage of occurrence as a function of the frequency for each type, are plotted as stacked curves in Fig. 8.

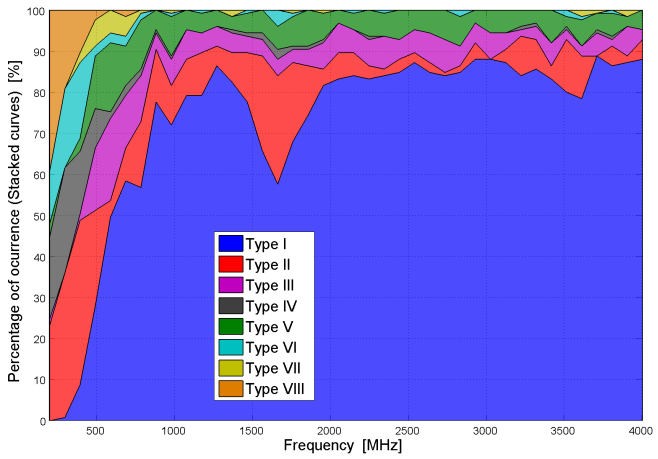

Fig. 8. (color online) Marginal PDFs types percentage of occurrence over frequency bins. The eight curves are plotted stacked on one another.

It can be seen on Fig. 8 that the occurrence of Type I statistics (the ideal case), starts to rapidly grow right in the region were the LUF was defined (three to six times the cutoff frequency f_{110}). After this point, the occurrence of Type I is rather constant and dominant, yet never absolute. It is observed that even in high frequency regime some anomalous statistics occur with a rate of approximately 15-20% (and it reaches even 40% for some particular circumstances, like at 1500 MHz).

It is also to be noticed that the contribution of Type II statistics (which coincides with the Rice distribution for the case of the magnitude) seems also to be relatively constant all along the measured frequency band.

In the undermoded region our model can not be rigorously applied, since the different hypothesis tests performed assume a normal distribution of the data samples, which is only the case in the overmoded region. Nevertheless, it is interesting to note that there is a dominance of even Types occurring in the undermoded region, while the opposite takes place in the frequencies after the LUF, where the odd Types prevail (despite Type II that, as was mentioned, is constantly present all along the band).

Furthermore, it appears from our measurements that the occurrence of the Types accounting the largest number of deviations from ideality i.e. Type IV, VI, VII and VIII is rather scarce in the overmoded region, being more dominant the Types with only one (or none) deviations from ideality i.e. Type I, II, III and V.

VI. Conclusions

In the present work, we reported on a statistical analysis of "good-but-imperfect" reverberation in an empty VIRC. Measurements were performed over a relatively wide band including both the undermoded and the overmoded regimes. Our considerations are focused mainly in the overmoded regime.

The Anderson-Darling Goodness-of-Fit test has been employed to detect an inconsistent rejection rate between data assessed using the real and imaginary parts of the complex field and using the magnitude and phase of the same field. Rejection rates for the underlying gauss-normal variates show to be lower than the rejection rates for the Rayleigh and Uniformly distributed magnitude and phase, respectively. This fact help us exclude sampling as a main cause for anomaly occurrence. It was discussed how the step from two gaussian random variables into a Rayleigh and a Uniform random variables is done assuming certain conditions of ideality. By relaxing these assumptions we showed a richer family of PDFs that are able to account for the statistics of the deviations from ideality.

Moreover, by means of this statistical model, we are able to not only detect but also to classify the anomalies occurring in the VIRC.

The results reported in this paper are to be helpful in better understanding the behavior of resonant fields in enclosed reverberant environments, where non-ideal random fields are present.

Acknowledgements

The research leading to these results has received partial funding from the European Community's Seventh Framework Programme - HIRF-SE project - under grant agreement number 205294 and partial funding from the Sixth Framework Programme - PEM project - under grant agreement number 042707.

References

[1] D. Hill: *Electromagnetic Fields in Cavities: Deterministic and Statistical Theories*, Piscataway, IEEE Press, 2009.

[2] F. B. J. Leferink, J.-C. Boudenot, W. van Etten: "Experimental results obtained in the vibrating intrinsic reverberation chamber", *IEEE International Symposium on Electromagnetic Compatibility*, vol. 2, pp. 639-644, August 2000.

[3] R. Serra, F. Canavero: "Bivariate Statistical Approach for Good-but-Imperfect Electromagnetic Reverberation", accepted for publication in *IEEE Transactions on Electromagnetic Compatibility*, October 2010.

[4] R. Serra, F. Leferink: "Optimizing the Stirring Strategy for the Vibrating Intrinisic Reverberation Chamber", *International Symposium on Electromagnetic Compatibility (EMCEurope 2010)*, Wrocław (Poland), September 13-17, 2010.

[5] J. G. Kostas and B. Boverie: "Statistical model for a mode-stirred chamber", *IEEE Transactions on Electromagnetic Compatiblity*, vol. 33, pp. 366-370, 1991.

[6] A. Papoulis: *Probability, Random Variables, and Stochastic Processes*, New York, NY: McGraw-Hill, 1965.

[7] CISPR/A and IEC SC 77B: IEC 61000-4-21 Electromagnetic Compatibility (EMC) - Part 4-21: Testing and Measurement Techniques - Reverberation Chamber Test Methods, International Electrotechnical Commission (IEC) International standard, August 2003.

[8] C. Lemoine, P. Besnier, M. Drissi, "Investigation of Reverberation Chamber Measurements Through High-Power Goodness-of-Fit Tests", *IEEE Transactions on Electromagnetic Compatibility*, vol. 49, no. 4, pp. 745-755, November 2007.